

# 3-3-4 Using a Neural Network to Make Operational Forecasts of Ionospheric Variations and Storms at Kokubunji, Japan

NAKAMURA Maho, MARUYAMA Takashi, and SHIDAMA Yasunari

An operational model was developed for forecasting ionospheric variations and storms at Kokubunji (35° N, 139° E), 24 hours in advance, by using a neural network. The ionospheric critical frequency (foF2) shows periodic variabilities from days to the solar cycle length and also shows sporadic changes known as ionospheric storms caused by geomagnetic storms (of solar disturbance origin). The neural network was trained for the target parameter of foF2 at each local time and input parameters of solar flux, sunspot number, day of the year, K-index at Kakioka. The training was conducted using the data obtained for the period from 1960 to 1984. The method was validated for the period from 1985 to 2003. The trained network can be used for daily forecasting ionospheric variations including storms using prompt daily reports of K-index, sunspot number, and solar flux values available on-line.

## **Keywords**

Ionosphere, Ionospheric storm, Neural network, Geomagnetic index

## **1 Introduction**

As of 2010, solar activity passed the turning point of the minimal period and became active again toward the next maximal period. In solar maximum, explosive phenomena such as solar flares often occur on the sun's surface and disturb the earth's magnetosphere and ionosphere. The ionosphere—a vast plasma region spreading from an altitude of about 80 km to 1000 km—has been utilized by humans as a reflective layer for radio communications using short-wave propagation. In recent years, space shuttles and numerous satellites have been orbiting in and above the ionosphere. As satellite signals reach the ground passing through the ionosphere, fluctuations of ionospheric electron density resulting from solar activity significantly influence satellite signals utilized for such purposes as satellite positioning systems.

A drastic fluctuation in ionospheric elec-

tron density is called an ionospheric storm, which is classified into two types: a negative phase ionospheric storm (negative storm) having reduced density, and a positive phase ionospheric storm (positive storm) having increased density. The mechanism of negative storms is considered as follows: Thermal expansion of the thermospheric neutral atmosphere is caused by energy flowing into the polar region, thereby changing the altitude distribution of neutral atmospheric particles, and increasing nitrogen molecules (N<sub>2</sub>) to exceed the mass of oxygen molecules (O) when the temperature rises at ionospheric altitudes, resulting in a larger ionospheric recombination coefficient and thus reduced electron density [1]. On the other hand, the mechanism of positive storms cannot be explained by the N<sub>2</sub>/O ratio; ionospheric plasma moves to higher altitudes for some reason, resulting in reduced N<sub>2</sub> density and thus the recombination coefficient becomes low. While ionization progresses

during the daytime, ionospheric plasma is supplied to high altitudes from an altitude of about 180km, where the production rate is high, resulting in an increased F-layer electron density[1]. The rises in ionospheric altitude are mainly considered caused by two reasons: upward movement perpendicular to magnetic field lines produced by the  $\mathbf{E} \times \mathbf{B}$  drift due to an eastward electric field originating in the magnetosphere[2], and upward movement parallel to magnetic field lines produced through the collisions of neutral atmospheric particles with ions due to thermospheric wind within the horizontal plane as directed from the polar region toward the equator[3]. However, the accurate forecasting of ionospheric storms including negative and positive phases has yet to be realized due to the difficulty of steady observations of the upper atmosphere. Our study targeted the development of a practical system for empirically forecasting ionospheric fluctuations including ionospheric storms by using a neural network with inputs of solar activity and geomagnetic activity indices.

The artificial neural network (NN) is a calculation algorithm that models the cranial nerves of animals and in recent years has been used in wide-ranging areas as a mechanism suited for extracting the characteristics of a complex phenomenon. The NN can learn the relation between inputs (consisting of multiple elements as the reasons for a given phenomenon) and outputs resulting from that phenomenon (functional approximation capability)[4]. With many candidate inputs possibly listed due to the complexity of ionospheric fluctuations as natural phenomena, learning by the NN requires data with qualitative stability over an extended period. Moreover, some sorting out or other ingenious means may be necessary to a certain extent for handling larger amounts of data that entail more time needed for learning. Both sunspot number and solar flux (indicators of periodic fluctuations in solar activity) are used as inputs of the factors of periodic ionospheric fluctuations caused by solar activity. Since ionospheric storms have been known in most cases to occur by

responding to magnetospheric disturbances, this study also used the K-index—a geomagnetic activity index indicating magnetospheric fluctuations—as part of the inputs.

Section 2 below describes the configuration and learning algorithm of the multi-layer NN used for learning and the inputs/outputs; Section 3 presents the learning and evaluation results. In addition, Section 4 introduces operation of the newly developed forecasting system and Section 5 summarizes this study.

## 2 Constructing a NN model for forecasting ionospheric fluctuations

### 2.1 Multi-layer perceptron and back propagation method

We used a 3-layer perceptron of the feed forward type in this study. Figure 1 illustrates the NN configuration. The following explains the scheme for learning by the NN. The teach signals and input elements in the learning will be discussed in detail in the next section or later.

The 3-layer perceptron has a so-called hidden layer between the input and output layers, with all units in one layer being combined with all units in the adjacent layer. Each unit has a respective weight, and the learning is performed by making weight adjustments.

The learning algorithm used is referred to as the back propagation method, where a combination of weights is determined through repetitive learning so that the square sum of errors in the target signals and outputs is minimized for combination. The adjusted amount of weights is then back-propagated from output to input during the learning process in order to update the NN. The following shows the algorithm of the back propagation method. Note that there may generally be more than one output, although the NN configured for this study only includes one output. The algorithm shown below is intended for multiple numbers ( $m$ ) of outputs[5].

Assume that every unit has the weight of  $\omega$  in the network with  $n$  inputs and  $m$  out-

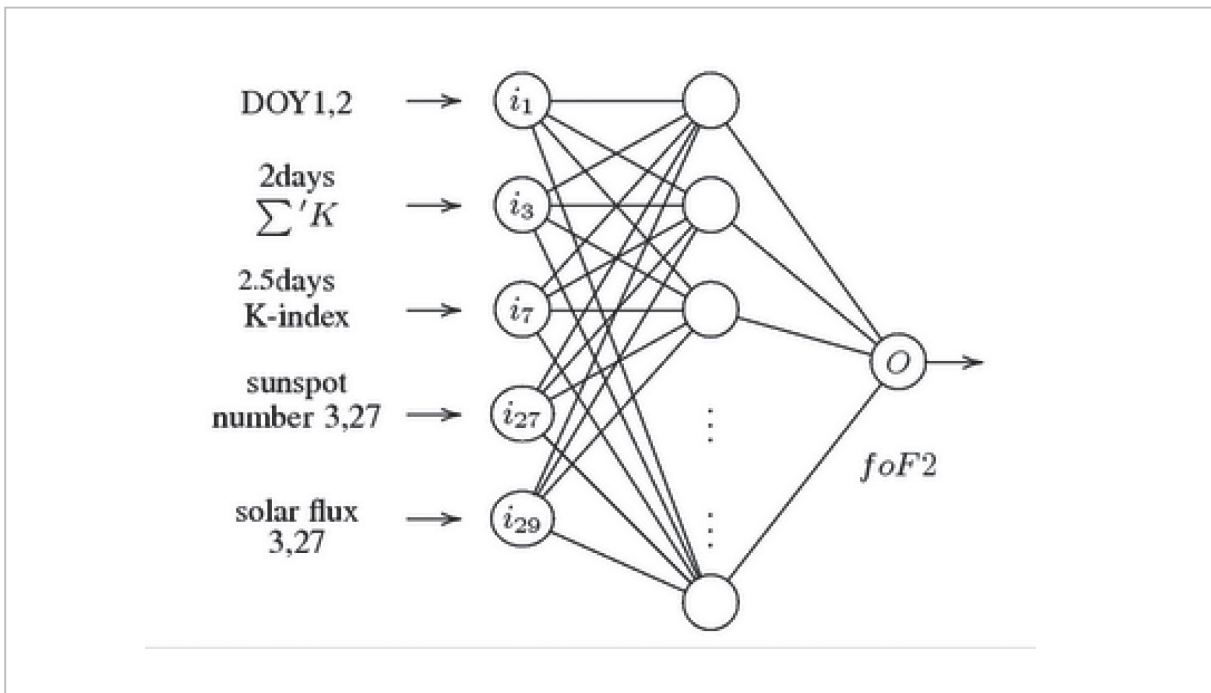


**Fig. 1** Configuration of the neural network

puts. In addition, a unit referred to as threshold element is adopted for input as the  $(n+1)$ th element.

1. Initialize values of all weights  $\omega_{ji}$  ( $i = 1, \dots, n+1; j = 1, \dots, m$ ) to random small values. Learning rate  $\eta$  ( $0 < \eta \leq 1$ ) is also set.
2. Target output  $t_p = (t_{p1}, \dots, t_{pm})$  and corresponding input pattern vector  $i_p = (i_{p1}, \dots, i_{pm}, 1)$  are given.
3. Using given weight  $\omega_{ji}$  ( $i = 1, \dots, n+1; j = 1, \dots, m$ ) and input pattern vector  $i_p$ , the output of each unit from the input layer toward the output layer is calculated as follows:

$$O_{pj} = f \left( \sum_{i=1}^{n+1} \omega_{ji} i_{pi} \right), j = 1, \dots, m$$

Note that  $f$  is a logistic function.

4. Using determined output  $O_{pj}$  and target output  $t_{pj}$  ( $j = 1, \dots, m$ ), error  $\delta_{pj}$  of unit  $j$  corresponding to pattern  $p$  is calculated from the output layer toward the input layer. Error  $\delta_{pj}$  is classified as a unit either for output or the hidden layer, and each  $\delta_{pj}$  is determined as follows:

Unit for the output layer:

$$\delta_{pj} = \beta o_{pj} (1 - o_{pj}) (t_{pj} - o_{pj}),$$

Unit for the hidden layer:

$$\delta_{pj} = \beta o_{pj} (1 - o_{pj}) \left( \sum_k \delta_{pk} \omega_{jk} \right)$$

$\sum_k$  is given as the sum of errors for all units  $k$  of the next layer to which unit  $j$  sends the outputs.

5. Using corrective amount  $\Delta_p \omega_{ji} = \eta \delta_{pj} o_{pj}$  of the weight, weight  $\omega_{ji}$  is corrected for each layer from output layer toward input layer as follows:

$$\omega_{ji} \leftarrow \omega_{ji} + \Delta_p \omega_{ji}$$

6. The learning is deemed completed when squared error  $E$  for all learning patterns is equal to or less than the set value. Otherwise, steps 2 to 5 are repeated for all learning patterns.

## 2.2 F2 layer critical frequency (foF2) as a target signal

The critical frequency of the F2 layer (foF2), a parameter that expresses the state of

ionospheric fluctuations, is used as the teach signal of the NN in this study. Note that foF2 is also a parameter given by observations using a vertical sounder called an ionosonde (Fig. 2), and is one of the parameters read from ionograms (Fig. 3) produced from ionosonde observations. The ionogram shows an altitude profile of ionospheric electron density, where the reflective altitudes of radio waves swept by radar are plotted with the lateral and vertical axes denoting frequency and altitude, respectively. Ionosonde observation has a history of over 50 years at four locations in Japan: Wakkanai, Kokubunji, Yamagawa and Okinawa.

Figure 4 shows the general behavior and periodic fluctuations of foF2. In this figure, plotting is made using the foF2 observational data, sunspot numbers, and solar fluxes for the 14 years from 1990 to 2004. It is obvious from the figure that the sunspot number and solar flux correlate with long-term fluctuations in

foF2. Note that foF2 peaks in spring and autumn, and increases in the maximal period of solar activity up to several times the level in the minimal period.

A 15-minute ionosonde observation yields 96 foF2 data items per day, and we used an hourly value (of 24 foF2 data items per day), since learning requires data over a span of at least 20 years. Here, foF2 was extracted from the data given by ionograms for the period from 1960 to 2002[6] and values normalized with the maximum value in the period was used for learning.



Fig.2 10C type ionosonde transceiver

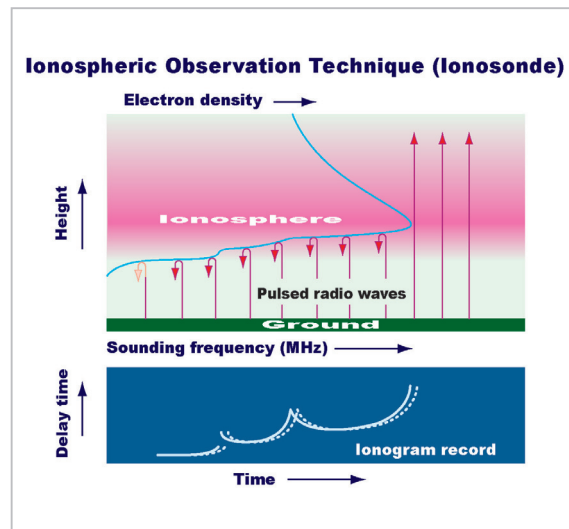


Fig.3 Scheme of ionospheric observation

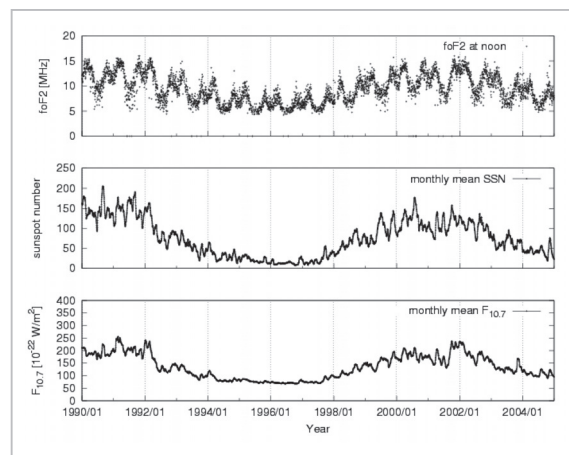


Fig.4 Long-term ionospheric fluctuations

## 2.3 Input parameters

Periodic fluctuations in the ionosphere can roughly be considered a superposition of three components of cyclic fluctuations: 11-year fluctuations due to the 11-year solar cycle, seasonal fluctuations, and daily fluctuations due to solar irradiation. Geomagnetic fluctuations causing ionospheric storms must also be input for the NN in addition to these three cyclic fluctuations. The following describes the input parameters and numerical processing performed for learning in detail.

### 2.3.1 Sunspot number

Solar activity fluctuates in a cycle of about 11 years and entails fluctuations of extreme ultraviolet (EUV) solar radiation, which contributes to the production of F-layer ionospheric electron density. Thus, the ionosphere is significantly influenced by solar activity. There is also the sunspot number as an index for indicating solar activity. Such phenomenal activity as a solar flare or coronal mass ejection (CME) is known to occur at places subject to the sun's intense magnetic field (known as sunspots). Multiple sunspots often appear in a state of gathering (referred to as sunspot group). Sunspot relative number  $R$  is defined by using  $f$  to denote the total number of sunspots existing in all sunspot groups visible on the entire surface of the sun,  $g$  the number of sunspot groups, and  $k$  the coefficient for compensating for variances caused by observers and/or telescopes as follows:

$$R = k(10g + f) \quad (1)$$

In the solar activity cycle of about 11 years, a period with maximum  $R$  is referred to as the solar maximum, and that with minimum  $R$  as the solar minimum.  $R$  fluctuates not only in the 11-year solar cycle but also in a 27-day cycle due to the sun's rotation. The observed sunspot number is quantitative data consistently accumulated according to evaluation equation (1) since more than 300 years ago, and high accuracy regarding the cyclic nature of sunspot number fluctuations is statistically guaranteed[7]. Thus, the NN uses the sunspot

number as one item of input data. To prepare input data for this study, one data item per day since 1960 was taken[8] with its normalization made with the maximum value in the period from 1960 to 2002. Since the learning did not satisfactorily converge with the daily data, smoothing was done using the numerical values of 3 and 27 days before each subject day, in order to use the two resultant sunspot numbers for input.

### 2.3.2 Solar flux

Another index for indicating solar activity is solar flux ( $F_{10.7}$ ), which is defined as the intensity of solar radio waves having a wavelength of 10.7 cm (2800 MHz) showering the earth as measured at Ottawa, and indicated in units of  $10^{-22}$  (W/m<sup>2</sup>Hz). One observational data item per day of solar flux ( $F_{10.7}$ ) can be taken. To prepare inputs, we also employed the  $F_{10.7}$  data since 1960[9] and normalized that data with the maximum value. Similarly to the case of sunspot numbers, large fluctuations only appeared when using the daily data and learning did not satisfactorily converge. A good convergence resulted from taking 3- and 27-day averages to smooth the data and using the results for input.

### 2.3.3 Seasonal fluctuations

The second most significant factor of ionospheric fluctuations following solar activity is seasonal fluctuations. Changes in the amount of incoming solar irradiation due to the positional relation of latitude/longitude with the sun significantly affect generation of the ionosphere. The *Day of Year (DOY)* is used for inputting seasonal fluctuations. The repetitive use of *DOY*—consisting of 1 to 365 days (or 366 days)—results in a drastic drop at the return from 365 to 1. To avoid such discontinuity of data, two input data items (*DOY 1* and *DOY 2*) were prepared as shown below, along with respective *sin* and *cos* calculations. In addition, each input was normalized to fall within the range of 0 to 1 in order for the NN to learn.

$$DOY 1 = \frac{\left( \sin\left( doy \cdot \frac{\pi}{180} \right) + 1 \right)}{2}$$

( $doy = 1, 2, \dots, 365$ )

$$DOY 2 = \frac{\left( \cos\left( doy \cdot \frac{\pi}{180} \right) + 1 \right)}{2}$$

( $doy = 1, 2, \dots, 365$ )

### 2.3.4 Daily fluctuations

To incorporate daily fluctuations due to solar irradiation into inputs, learning was performed with each local one-hour value, as classified into 24 values. The learning periods were independent of each other. The output data were arranged in order of time for execution, and normalized with the maximum value in the learning period at each one-hour value for learning.

### 2.3.5 Geomagnetic activity K-index

Cyclic fluctuations due to solar activity and seasonal fluctuations are considered reproducible by using solar observational data and *DOY* input. However, for accidental fluctuations such as ionospheric storms, geomagnetic fluctuations causing such storms must be added to the inputs. There is a delay of about one to two days for an accidental solar fluctuation to reach and influence the earth's ionosphere by passing through the magnetosphere. By using this delay, learning information about one day before in the NN enables forecasting.

A variety of geomagnetic activity indices have been proposed and used by geomagnetic observatories covering the entire world to quantitatively capture various magnetospheric disturbances. There are wide-ranging indices such as the AE index for monitoring aurora behavior in the polar region, Dst index for indicating ring currents developed during magnetic storms, ap index for indicating the level of geomagnetic activity in the mid-latitude region, and Kp index linearly converted from the ap index<sup>[10]</sup>. The Kp index averages the K-index, a local geomagnetic activity index for various regions, and has been widely

used as an index for indicating geomagnetic activity of the entire earth. In addition, the Kp index is considered suitable as input for learning, since this index can monitor the occurrence of geomagnetic disturbances that produce ionospheric fluctuations. In fact, many studies on ionospheric fluctuations conducted in Europe have actually used the ap or Kp index<sup>[12]-[14]</sup>. However, these indices lack promptness and require much time for fixing values. In contrast, among the K-indices used for determining the Kp index, the Kakioka K-index<sup>[15]</sup> observed at the Kakioka Geomagnetic Observatory in Japan shows promptness where its preliminary figures for each day are announced the next morning to enable early use as inputs for forecasting. Targeting the construction of a more practical forecasting system, we decided to use the K-indices as inputs of geomagnetic activity indices. In addition, as the AE index reflects energy flowing in from the magnetosphere more sensitively than the K or Kp index, it should essentially be included in the inputs. However, there is an insufficient period for the database to accumulate the AE index as provisional values. Thus, we did not use the AE index since the learning required for the NN may be degraded. Once a sufficient amount of data is accumulated over several years, the AE indices may be used as inputs.

The K-indices indicate the degree of geomagnetic disturbance in integers from 0 to 9, with eight points of the daily indices being calculated every three hours in universal time. Note that the component of daily fluctuations remains included in the Kakioka indices<sup>[16]</sup> (but removed from the Kp indices due to averaging), and 20 K-indices equivalent to 2.5 days were used as inputs for learning by the neural network. Numerical values normalized with the maximum number of 9 were used for learning. In addition,  $\Sigma K$  or the sum of eight K-indices for a given day has been used to indicate disturbances during a given day. Table 1 shows the relation of  $\Sigma K$  with the degree of geomagnetic disturbance proposed by the Kakioka Geomagnetic Observatory<sup>[17]</sup>.

**Table 1** Degree of geomagnetic disturbance and  $\Sigma K$

Geomagnetic disturbance level	$\Sigma K$
quiet	under 6
rather quiet	7 to 11
normal	12 to 17
minor storm	18 to 23
extreme storm	over 24

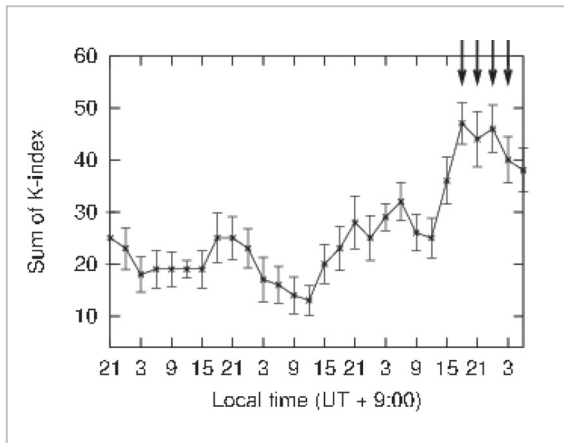


**Fig.5** Superposition analyses of geomagnetic K-index fluctuation patterns prior to a large ionospheric storm

$\Sigma K$  well expresses the degree of geomagnetic disturbance. However, it is known that the influences of geomagnetic fluctuations on the ionosphere vary depending on local time[1]; therefore, in order to effectively incorporate the local time dependence into inputs of this study, we extracted 10 examples of large ionospheric storms that occurred in the past and conducted superposition analyses for patterns of geomagnetic fluctuations known to have caused ionospheric storms. Figure 5 shows the results. The horizontal axis represents local time and a superposition is made for fluctuation patterns of K-indices for 3.5 days prior to the occurrence of ionospheric storms. The vertical axis represents the sum of

totalized K-indices and error bars are used to indicate standard deviation for the number of events. The results of analyses indicate that the fourth to seventh K-indices (indicated by arrows) from the previous day to the day when an ionospheric storm occurred exceed the normal level. Based on these results, we decided to split the eight K-indices at eight points in a day into two for use as inputs: the sum of indices corresponding to four points (4th to 7th) in a day and the sum of indices corresponding to the 8th point in said day, including the 1st to 3rd points the next day. The K-index resulting from this summing process is defined as  $\Sigma'K$ , which is equivalent to the two days added to the inputs for learning. Note that  $\Sigma'K$  was also normalized with the possible maximum value of 36.

## 2.4 Configuration of the networks and learning parameters

The network was structured in three layers with a total of 30 inputs and one output, and one-hour value of foF2 was used for a target signal. A total of 24 NNs were configured for each time division for learning, and outputs from each NN were arranged in order of time for execution. Note that small initial values of weight were set in the range from  $-0.5$  to  $0.5$  by using random numbers.

Once inputs and outputs were determined, a network could be configured. For actual learning in the NN, however, learning parameters must be properly set in order for the learning to converge. Some parameters were available regarding the learning momentum to determine learning speed, number of data patterns used for learning, and number of hidden layers in the network. These parameters were determined based on learning being executed a number of times with a review made after each execution on a trial-and-error basis. Table 2 summarizes the learning parameters used in this study.

The termination of learning may be determined when the learning error drops below the set value[5]. However, in actual learning, reviewing only the error does not provide a

**Table 2** Learning parameters

<i>learning rate</i>	0.32
<i>learning momentum</i>	0.02
<i>number of patterns</i>	8760
<i>number of units in the hidden layer</i>	200

basis for judging whether learning is proceeding in good condition. As such, we set a target learning error to a very small value and ran many cycles of learning while monitoring the processes of square and generalization errors during the learning process. The generalization error is defined as a square error for data not used for learning, thereby functioning as an index of generalization capability of the learning process. As learning proceeded, the square error was gradually and steadily reduced to converge with a certain value, while the generalization error relative to an observational value generally increased from a certain point. The latter phenomenon is known as over-learning, where the capability of generalizing unlearned data is considered deteriorated. For execution, we used the weight at the point where the generalization error began increasing during learning in each local time (LT) and recorded the number of learning cycles at that point as the cycle providing the best learning results. There were about 7,000 cycles of learning based on such a manner for the entire time zone.

### 3 Results of learning and its evaluation

To review the reproducibility of periodic fluctuations due to solar activity, the results of learning about fluctuations are described in terms of several tens of years, seasons, and days (as described in Section 3.1), and their errors are compared with those given by the results from the IRI empirical model for the

ionosphere (described in Section 3.2). In addition, reproduced examples and forecasting scores including the negative/positive phases of ionospheric storms are described (in Section 3.3).

#### 3.1 Reproducibility of periodic fluctuations

##### 3.1.1 Reproducing long periodic fluctuations (11-year solar cycle)

First, Fig. 6 shows a reproduced long-term fluctuation. This figure also compares one-hour observational value of foF2 (shown in the middle) with outputs of one-hour value from the NN (shown at the bottom) for the period of 1985 to 1996, from which no data was picked for learning. Moreover, the average fluctuation over three days is also shown at the top in terms of sunspot number (solid line) and solar flux (dotted line). The outputs from the NN well reproduced the fluctuations of the observational foF2 in synchronism with the approximative 11-year cycle of solar activity. In addition to this 11-year cycle, it is also obvious that annual and seasonal fluctuations are reproduced. Note that outputs from the NN show less scattering of values compared to observational values. This implies that the NN cannot necessarily follow extreme increases or decreases in values, which may occur at such abnormal events as ionospheric storms.

##### 3.1.2 Reproducing seasonal and daily fluctuations

Figure 7 is presented to review the reproducibility of seasonal and daily fluctuations with data plotted for seven days. In this figure, the data of a relatively quiet seven days in terms of geomagnetic activity were selected and extracted from 1992 (right column) as the solar maximum period, and from 1985 (left column) as the minimum period for March (top), August (middle) and October (bottom), thereby allowing a comparison to be made by focusing on observational values (dotted line) and outputs from the NN (blue solid line). It is obvious from the figure that normal values in both maximum and minimum periods are well reproduced with the NN for each season.

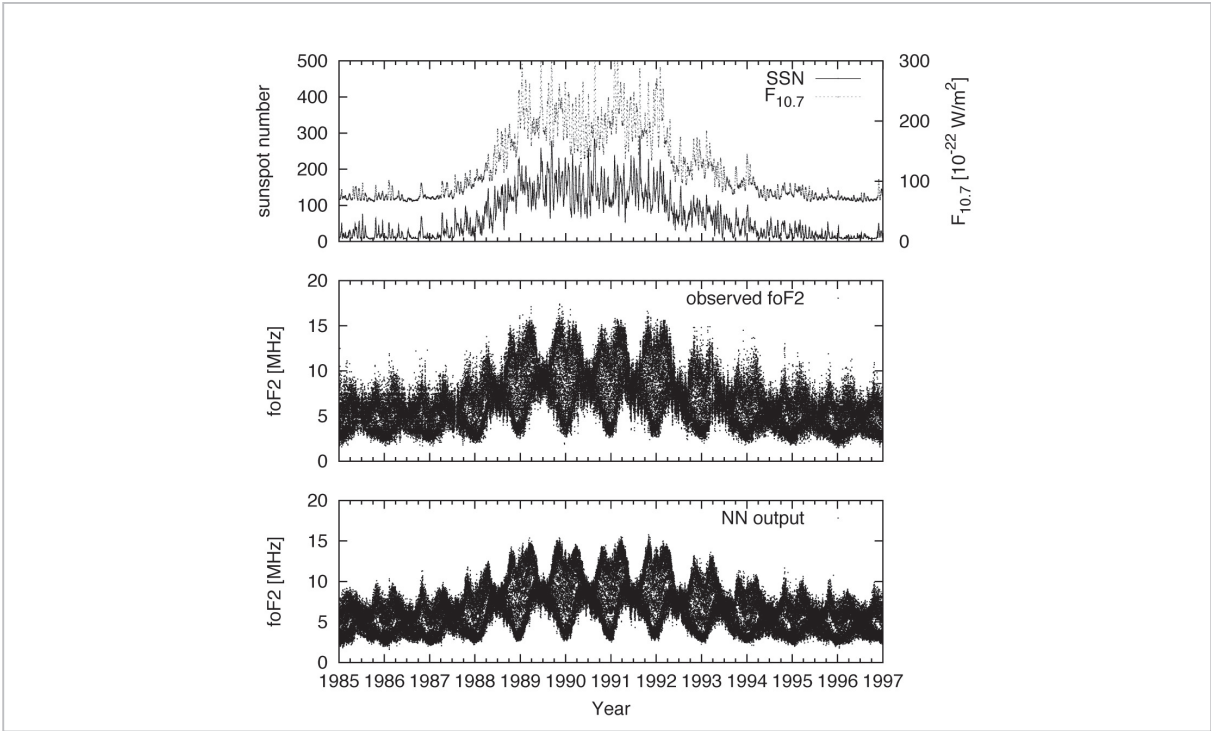


**Fig.6** Reproducing long cyclic fluctuations

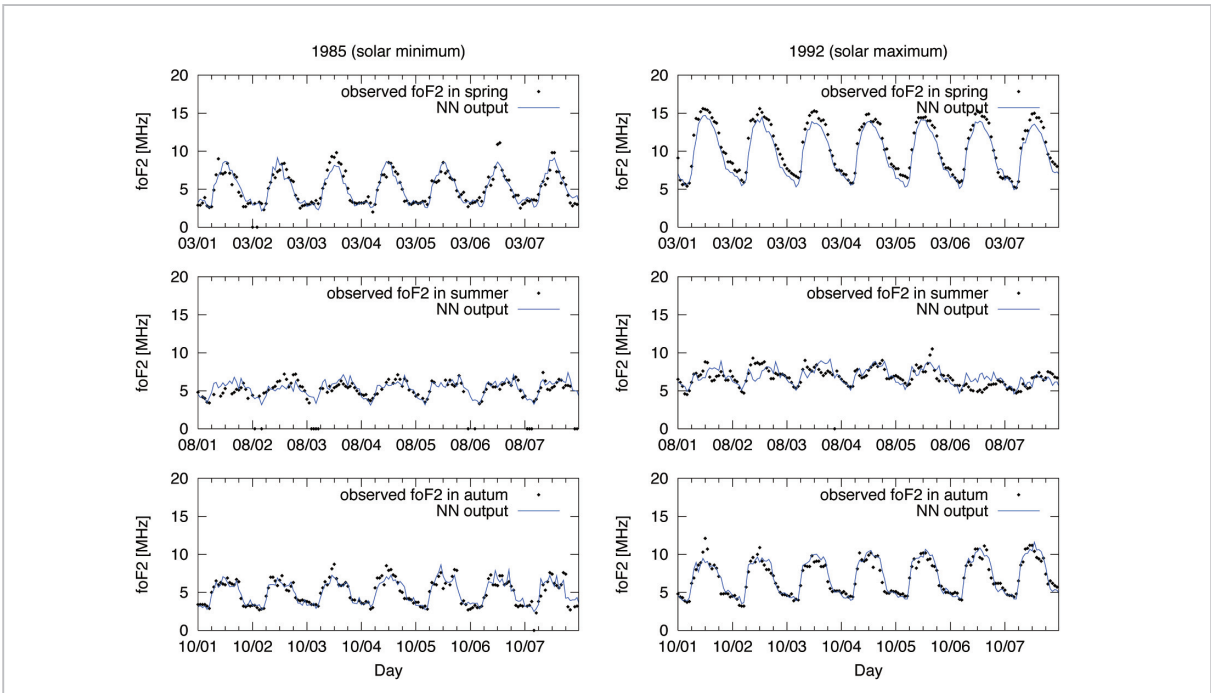


**Fig.7** Reproducing seasonal and daily fluctuations

### 3.2 Comparison with an empirical model (IRI)

A comparison was made relative to a commonly used empirical model known as international reference ionosphere (IRI)[18]. IRI

uses a geomagnetic index referred to as the ap index instead of the K-index for indicating magnetospheric influences. By using IRI, we prepared outputs with an identical one-hour value for the same period as for the NN (1985

to 1996). By using both methods, we compared square errors of outputs from the NN and IRI in the same period to actual observational values. First, correlation coefficients with respect to the observational values were calculated and compared for each year during the period (Fig. 8). The correlation coefficient for outputs from IRI dropped to 0.76 due to large errors in the solar maximum period, while the coefficient for those from the NN constantly remained above 0.92 through both maximum and minimum periods.

Next, the square errors for each LT were compared in the maximum and minimum periods (Fig. 9).

According to Fig. 9, reproduction by the

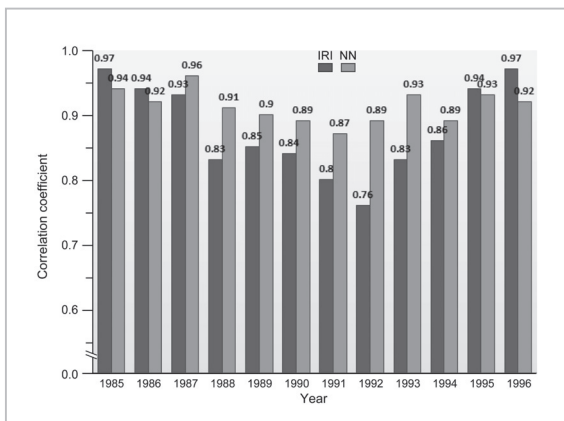


**Fig.8** Comparison of correlation coefficient between NN outputs and observational values with that between the IRI model and observational values for 12 years (one solar cycle)

NN is considered better in terms of accuracy than that by IRI in most time periods in spring and autumn during both maximum (left column) and minimum (right column) periods. The electron density is highest in spring and autumn during the year. There are large errors in outputs from IRI (upper level) in time periods around evening during both maximum and minimum periods. In contrast, no significant bias on errors due to local time is observed with outputs from the NN. The reasoning behind the error bias on IRI is considered a lack of observational data in Asia (including Japan).

### 3.3 Reproducing ionospheric storms

#### 3.3.1 Example of forecasting ionospheric storms

The following describes three successful examples of forecasting negative and positive storms. Figures 10 to 15 indicate forecasted storms for three days including the day on which an ionospheric storm occurred. The top levels in the figures indicate a transition in the K-index; the middle levels indicate observed foF2 (red dot), forecasted foF2 (blue dotted line), and the median value for 27 days before the observational day (black solid line). In addition, the bottom levels indicate the variance between values forecasted by the NN using actual K-indices and those forecasted under the assumption that geomagnetic activity quietly underwent a transition (where all

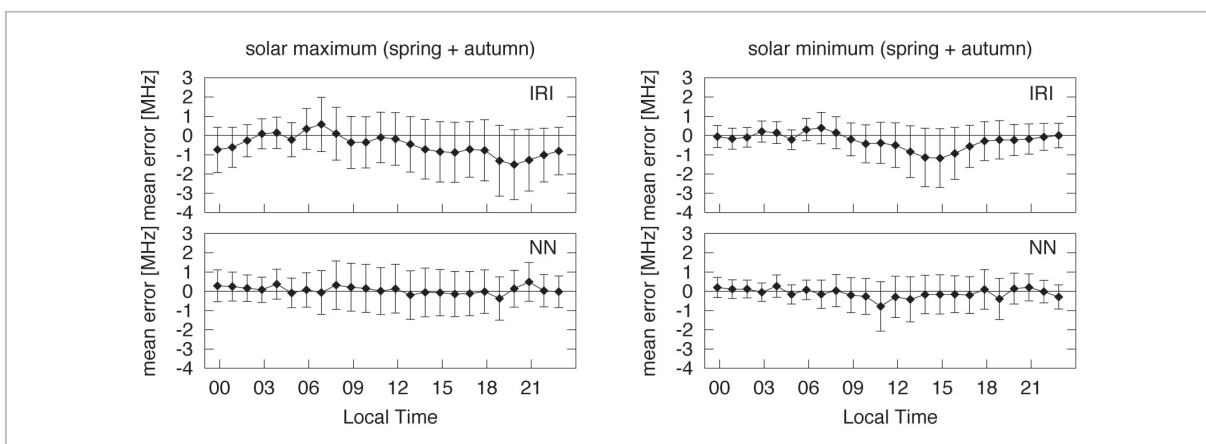


**Fig.9** Comparison of square errors in spring and autumn during maximal and minimal periods at local time for the NN and IRI model

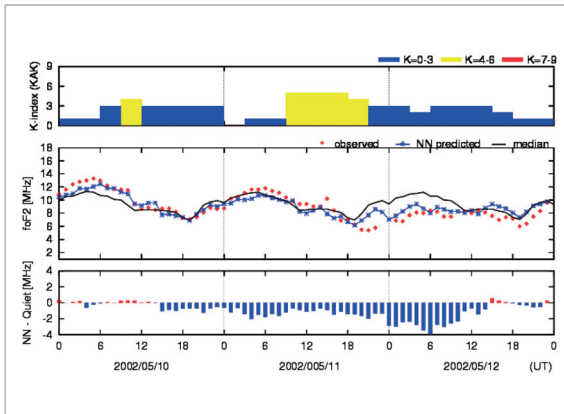


**Fig. 10** Example 1 with negative storms forecasted on May 12, 2002

The top level indicates the K-index; the middle level indicates the observational foF2 values (red dot), outputs (blue dotted line) obtained by the NN, and monthly median values of observational values (solid line); the bottom level indicates forecasted fluctuation by using variances relative to outputs when setting K to a constant value ( $K = 1$ ) in the NN, where red indicates an increasing trend of fluctuation from a quiet period, and blue indicates a decreasing trend. The same applies to other related figures.

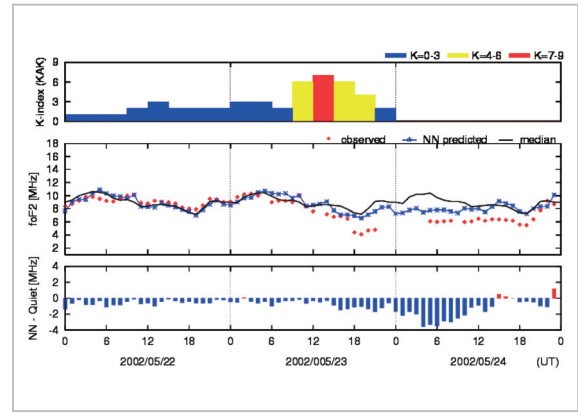


**Fig. 11** Example 2 with negative storms forecasted on May 24, 2002

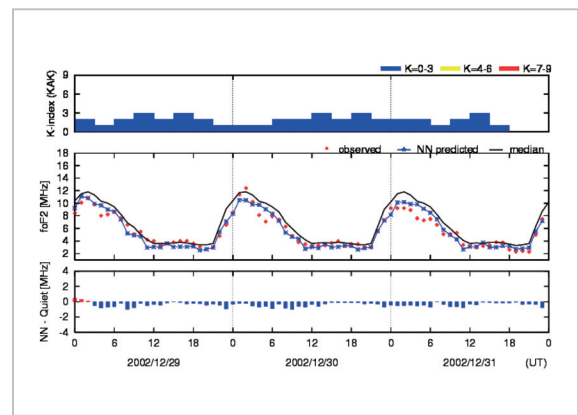


**Fig. 12** Example 3 with negative storms forecasted on December 31, 2002

inputs for K-indices become 1) during NN execution. Ionospheric storms forecasted as being reduced in number from a quiet period are indicated with blue bars, while storms forecasted as being increased in number are indicated with red bars.

Figures 10 to 12 show three examples of successfully forecasted negative storms. Figures 10 and 11 each show an example of forecasting an event, where a negative storm occurred two days after the occurrence of magnetic storms. In both examples, the K-indices underwent a transition with a value of 3 or more from the afternoon to evening of the second day. In Fig. 11, the fourth K-index (18:00 to 20:00 LT) increased to 6 and the fifth K-index (21:00 to 23:00 LT) to 7 on May 22, 2002. This coincides with the trend of magnetic fluctuation patterns on the day before and two days before as given by superposition analyses shown in Fig. 5. Figure 12 shows an example of relatively quiet negative

storms that occurred from December 29 to 31, 2002. The sum of daily K-indices ( $\Sigma K$ ) underwent a transition of 20, 16, 11 and 11 during the four days from December 28 through 31. The four-day  $\Sigma K$  implies relatively quiet disturbances according to Table 1, which shows the degree of geomagnetic disturbance proposed by the Kakioka Geomagnetic Observatory. Consequently, the forecasting is understood as being made for cyclic geomagnetic disturbances due to coronal holes occurring during an approximate 27-day cycle of solar activity.

Next, Figs. 13 to 15 show three examples of successfully forecasted positive storms. In the example for the period of November 20 to 22, 2002 (in Fig. 13), the K-index increased to 5 on November 20, with about the same level of geomagnetic disturbance being retained

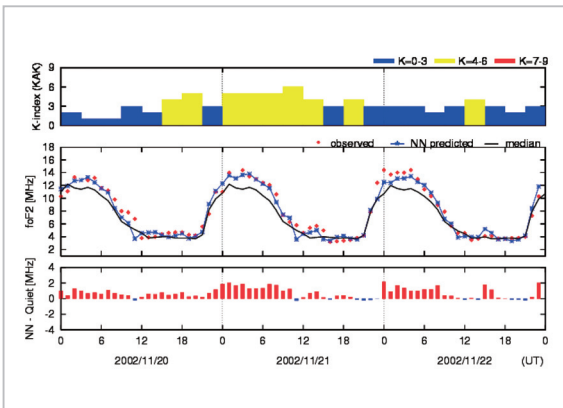


**Fig. 13** Example 1 with positive storms forecasted on November 22, 2002

The top level indicates the K-index; the middle level indicates the observational foF2 values (red dot), outputs (blue dotted line) obtained by the NN, and monthly mean values of observational values (solid line); the bottom level indicates forecasted fluctuation by using variances relative to outputs when setting K to a constant value ( $K = 1$ ) in the NN, where red indicates an increasing trend of fluctuation from a quiet period, and blue indicates a decreasing trend. The same applies to other related figures.

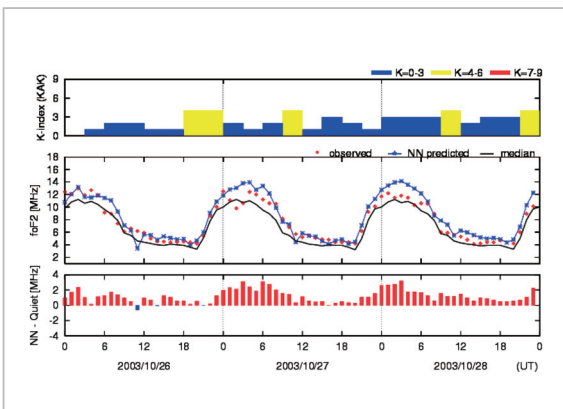


**Fig. 14** Example 2 with positive storms forecasted on October 28, 2003

over the next two days. Following these magnetic disturbances, positive storms occurred in the ionosphere for several days. Based on a comparison of median values (solid line) and observational values (red dot) shown in the middle of the figure, ionospheric electron density is understood as having only increased during the daytime and not at nighttime. Such local time dependence was also reproduced

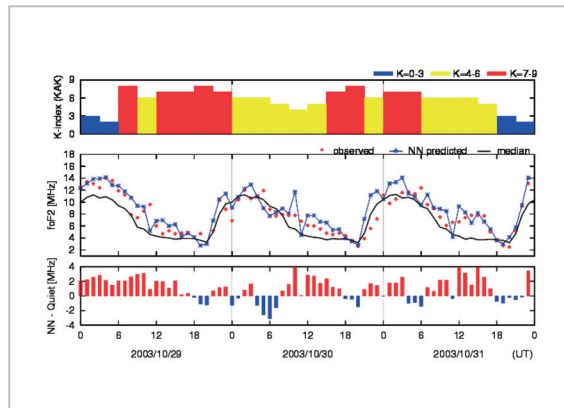


**Fig. 15** Example 3 with positive storms forecasted on October 31, 2003

well in the NN. Figures 14 and 15 show examples indicating magnetospheric and ionospheric disturbances that continued for three days after intense solar flares occurred on October 28, 2003. In this event, the intensity of solar flares reached abnormally high X17.2 on October 28, 2003 11:51 UT; and was later referred to as the “Halloween Event” due to these almost unprecedented magnetic storms in history. The magnetic disturbances then lasted until 6:11 UT (15:11 JST) on October 29[19]. Although the ionosphere was drastically disturbed in responding to these geomagnetic disturbances, the NN could forecast these disturbances very accurately over a wide range. Satellite positioning systems and similar systems were forecast as being influenced by such a drastic event due to the drastic disturbances or changes in ionospheric electron density. The NN is considered significant for constructing an ionospheric storm forecasting system, since it at least forecasted the occurrence of such drastic disturbances.

### 3.3.2 Score of forecasting ionospheric storms

To comprehensively discuss forecast accuracy, we newly introduced ionospheric disturbance index  $\delta_{\text{obs}}$ , the basis of which lies in observational values. Index  $\delta_{\text{obs}}$  is defined as the variance between the average and monthly mean values of foF2 taken from 6 a.m. until 6 p.m. on a given day. The days on which positive and negative storms occurred are defined as those with  $\delta_{\text{obs}}$  of 1 MHz or more and  $-1$

MHz or less, respectively. In addition, a day with  $0.6 \text{ MHz} \leq |\delta_{\text{obs}}| \leq 1 \text{ MHz}$  is specified as a semi-disturbance day and that within 0.6 MHz downwardly or upwardly beyond the range as a quiet day. Similarly, disturbance index  $\delta_{\text{NN}}$  is defined for outputs from the NN. Table 3 lists the relations between  $\delta_{\text{obs}}$  and  $\delta_{\text{NN}}$ . During the 11 years (4,383 days) used for the evaluation, negative storms were observed on 225 days, including 93 days forecasted by the NN as days of negative storms and semi-disturbance (negative), 13 days of positive storms and semi-disturbance (positive), and 119 days of no particular disturbance (quiet range). Conversely, positive storms were observed on 275 days, including 97 days forecasted by the NN as days of positive storms (including semi-disturbance), 20 days of negative storms, and 158 days of no disturbance. The results indicate a total of 3,179 quiet days, including 2,262 days forecasted within the range of 0.6 MHz. Thick characters in the table indicate the number of days correctly forecasted, or 2,488 days out of the total of 4,383 days (56.8%). The shaded cells indicate the days forecasted significantly incorrectly, or 661 days out of the 4,383 days (15.1%), and cells with thin characters on a white background indicate the days forecasted incorrectly but not significantly.

**Table 3** Accuracy of forecasting ionospheric storms

Obs \ NN	Obs				
	Negative	Weak Negative	Quiet	Weak Positive	Positive
Negative	48	32	112	12	9
Weak Negative	45	40	171	30	11
Quiet	119	191	2262	254	158
Weak Positive	10	22	463	81	40
Positive	3	4	171	38	57

## 4 Disclosing the forecasting system using the neural network

The following lists the functions required for practically forecasting ionospheric fluctuations.

- Providing latest (semi-real-time) information
- Automatically updating and disclosing data on websites
- Showing data of about three days to check the transition of ionospheric fluctuations
- Showing the observational and monthly median values, in order to check changes in values for normality and abnormality

To fulfill this requirement, we prepared a system that automatically acquired information on sunspot numbers[8], solar fluxes[9], and geomagnetic K-indices[15] from a website updated daily, and then added this information to a database as inputs for the neural network[20]. The neural network automatically accesses the databases once a day, executes forecasting and updating, and then updates the plots of forecasted values externally disclosed on the server. The system is currently disclosed on the website of the National Institute of Information and Communications Technology, Radio Propagation Project at <http://wdc.nict.go.jp/> (as shown in Fig. 16).

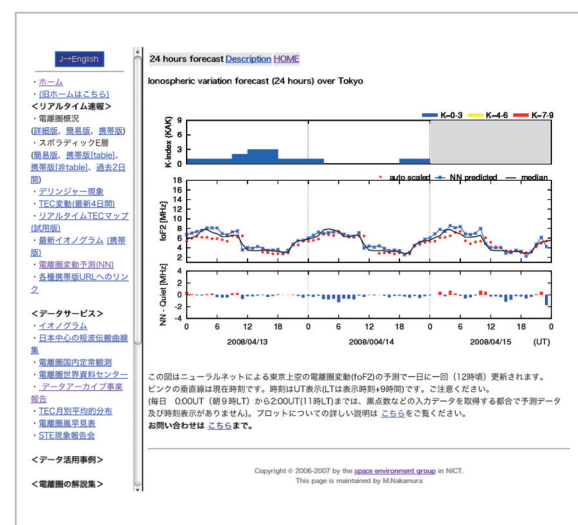


**Fig. 16** Website disclosure of ionospheric fluctuation forecasting

## 5 Conclusion

In this study, we constructed a system for forecasting ionospheric fluctuations about 24 hours ahead in the skies over Tokyo by using a neural network. We targeted constructing a system capable of practical use in the fields of short-wave and satellite communications by forecasting fluctuations 24 hours ahead, as well as accommodating normal cyclic fluctuations in the ionosphere and also accidental fluctuations in the negative/positive phases of ionospheric storms.

The ionospheric electron density is known to be determined by the balance between the generation of plasma due to extreme ultraviolet radiation and its elimination due to atmospheric chemical reactions involving significant solar activity. In addition, accidental disturbances such as chromospheric eruptions disturb the geomagnetosphere and trigger accidental fluctuations in the ionosphere. Based on these facts, ionospheric fluctuations equivalent to two cycles of solar activity (from 1960 to 1984) were learned by using a neural network provided with inputs of sunspot numbers and solar fluxes that represent solar fluctuations, and K-indices that represent geomagnetic activity. The neural network used the back propagation method of a 3-layer perceptron, where many trials were made on combinations of inputs and learning parameters, in order to determine the best suited learning. During the course of parameter adjustments, it became empirically apparent that many counts of learning were essential for stable learning by a large neural network, and that the final results of learning were largely affected by the sorting-out of input parameter combinations.

## References

- 1 G. W. Pröls, "Ionospheric F-region storms," Vol. 2 of Handbook of Atmospheric Electrodynamics, CRC Press, 1995.
- 2 N. Matuura, "Theoretical models of ionospheric storms," Space Sci. Rev., Vol. 13, pp. 124–189, 1972.
- 3 T. Maruyama, "4.4 Ionospheric storm," Wave Summit Course, Science of Space Weather, edited by K. Marubashi and T. Ondoh, Ohm-sya, 2000. (in Japanese)
- 4 K. Funahashi, "On the approximate realization of continuous mappings by neural networks," Neural Net-

We were able to improve the accuracy of forecasting ionospheric storms by newly defining and adding  $\Sigma K$  to the inputs used in this study. The learning was evaluated for a period (from 1985 to 1996) not used for learning. Consequently, learning was well executed with long-term fluctuations over a period of about 11 years due to solar activity, along with annual, seasonal and daily fluctuations, and a model was established with better accuracy than the commonly used IRI model. Ionospheric storms could also be forecasted, including increases or decreases in the electron density for many events. However, forecasting ionospheric storms also failed on many occasions, thereby requiring further improvements in forecasting probability. In the future, a system offering better accuracy in forecasting ionospheric storms should be constructed by using solar wind and time variations of geomagnetic storms as input data. A similar system should also be developed for the skies not only over Tokyo but also over the area stretching from Hokkaido to Kagoshima and Okinawa, where ionospheric observations are provided. Once realized, both systems are expected to be useful for modeling the ionospheric delay, and forecasting and establishing measures for disturbances in the growing field of satellite communications.

## Acknowledgments

We wish to thank our colleagues in the Space Environment Group and the staff at the World Data Center (WDC) for Ionosphere for providing the ionogram data, and the staff at the Kakioka Geomagnetic Observatory for providing the Kakioka K-indices.

- 
- works, Vol. 2, pp. 183–192, 1989.
- 5 S. Haykin, *Neural Networks: A Comprehensive Foundation*, Prentice Hall PTR, Upper Saddle River, NJ, 1994
  - 6 World Data Center for Ionosphere, 2000. <http://wdc-c2.nict.go.jp/>
  - 7 Memcalc, Questions and Answers. <http://www.gms-jp.com/MemCalcHP/4-1.htm>
  - 8 Pierre Cugnon, "SIDC RWC Belgium World Data Center for the Sunspot Index," 4 2002. <http://sidc.oma.be/index.php3/>
  - 9 Solar radio monitoring programme. <http://www.nrc-cnrc.gc.ca/eng/services/hia/radiomonitoring.html>
  - 10 World Data Center for Geomagnetism, Kyoto. <http://swdcwww.kugi.kyoto-u.ac.jp/wdc/Sec3.html>
  - 11 O. Altinay, E. Tulunay, and Y. Tulunay, "Forecasting of ionospheric critical frequency using neural networks," *Geophys. Res. Lett.*, Vol. 24, pp. 1467–1470, 1997.
  - 12 P. Wintoft and Lj. R. Cander, "Ionospheric foF2 storm forecasting using neural networks," *Phys. Chem. Earth*, Vol. 25, No. 4, pp. 267–273, 2000.
  - 13 L. A. Williscroft and A. W. V. poole, "Neural networks, foF2, sunspot number and magnetic activity," *Geophys. Res. Lett.*, Vol. 23, No. 24, pp. 3659–3662, December 1996.
  - 14 E. O. Oyeyemi, A. W. V. Poole, and L. A. McKinnel, "On the global short-term forecasting of the ionospheric critical frequency foF2 up to 5 hours in advance using neural networks," *Radio Sci.*, Vol. 40, No. RS6012, 2005, doi: 10.1029/2004RS003239.
  - 15 Kakioka Magnetic Observatory. <http://www.kakioka-jma.go.jp/>
  - 16 T. Yumura, "On the "three-hour-range indices" K at Kakioka," *Memoirs of the Kakioka Magnetic Observatory*, Vol. 6, pp. 1–17, 1951.
  - 17 K. Koike, "Statistics of the k-index," *Kakioka Magnetic Observatory, Gijutsu Hokoku*, Vol. 31, pp. 32–46, 1991.
  - 18 D. Bilitza, K. Rawer, L. Bossy, and T. Gulyaeva, "International reference ionosphere-past, present, future," *Adv. Space Res.*, Vol. 13, No. 3, pp. 3–23, 1993.
  - 19 M. A. Abdu, T. Maruyama, I. S. Batista, S. Saito, and M. Nakamura, "Ionospheric responses to the October 2003 superstorm: Longitude/local time effects over equatorial low and middle latitudes," *J. Geophys. Res.*, Vol. 112, No. A10306, 2007, doi: 10.1029/2006JA012228.
  - 20 M. I. Nakamura, T. Maruyama, and Y. Shidama, "Using a neural network to make operational forecasts of ionospheric variations and storms at Kokubunji, Japan," *Earth Planets Space*, Vol. 59, pp. 1231–1239, 2007.



**NAKAMURA Maho, Ph.D.**  
*Expert Researcher, Space-Time  
Standards Group, New Generation  
Network Research Center  
Ionosphere, Information Engineering*

**MARUYAMA Takashi, Ph.D. (Eng.)**  
*Executive Researcher  
Upper Atmospheric Physics*

**SHIDAMA Yasunari, Ph.D.**  
*Professor, Faculty of Engineering,  
Department of Computer Science &  
Engineering, Shinshu University  
Mathematical and Computational  
Analysis of Nonlinear Systems*